Residual resistivity as an independent indicator of resonant levels in semiconductors

Bartlomiej Wiendlocha, Shantanu Misra, Anne Dauscher, Bertrand Lenoir, Christophe Candolfi

Residual resistivity as an independent indicator of resonant levels in semiconductors

Bartlomiej Wiendlocha[1,,$], Shantanu Misra[2,$], Anne Dauscher[2], Bertrand Lenoir[2], Christophe Candolfi[2,+]*

[1] Faculty of Physics and Applied Computer Science, AGH University of Science and Technology, Aleja Mickiewicza 30, 30-059 Krakow, Poland
[*]E-mail: wiendlocha@fis.agh.edu.pl

[2]Institut Jean Lamour, UMR 7198 CNRS – Université de Lorraine, 2 allée André Guinier-Campus ARTEM, BP 50840, 54011 Nancy Cedex, France
[+]E-mail: christophe.candolfi@mines-nancy.univ-lorraine.fr

[$]Equal contributions

Distortion of the density of states induced by specific impurities, a mechanism known as resonant level (RL), is an efficient strategy to enhance the thermoelectric performances of metals and semiconductors. So far, experimental signatures identifying the resonant nature of an impurity have relied on the so-called Ioffe-Pisarenko plot that enables visualizing the induced thermopower enhancement at specific carrier concentrations. However, this method cannot solely discern RL from other possible band-structure-related sources of thermopower enhancement such as band-shape modifications or band convergence. An independent method of resolving this problem is proposed here. A detailed theoretical and experimental analysis of the low-temperature electrical resistivity ρ_0 and carrier mobility μ_0 of the resonant-level system SnTe doped with In is presented as a function of the impurity concentration x. By comparing to non-resonant cases of SnTe doped with I, Mn, and Ga, we demonstrate that the construction of $\rho_0(x)$ and $\mu_0(x)$ plots allows to distinguish between resonant and non-resonant impurities, even when some of them induce similar thermopower enhancements. This methodology is further confirmed by analyses performed for Na- and Tl-doped PbTe, illustrating how the combination of transport measurements at low temperatures can be used to determine the resonant nature of an impurity.

Introduction

Doping semiconductors with impurities is the cornerstone of modern electronics and conversion energy applications, providing a straightforward mean to tailor their electronic properties. Depending on the nature of the impurities, “rigid-like” or “non-rigid-like” with respect to the host semiconductor, their presence can induce either a mere shift in the chemical potential or more profoundly reshape the electronic bands. The electronic band structure of semiconductors can be thus advantageously manipulated by both types of impurities.

Among functional materials used in energy conversion technologies, thermoelectric semiconductors are a class of materials combining unique transport properties used in electrical power generators and Peltier cooling modules. The efficiency with which they directly convert heat into electrical power, and vice versa, at an absolute temperature T, is proportional to the figure of merit[1,2] $ZT = \alpha^2 T/\rho\kappa$, a dimensionless parameter that combines material-specific transport coefficients: thermopower α, electrical resistivity ρ and total thermal conductivity κ. Over the last decades, significant efforts were devoted to optimize the performance of thermoelectric materials via dedicated strategies focusing on either optimizing the power factor α^2/ρ through doping or lowering the total thermal conductivity κ.[3,4] In the former approach, band structure engineering has been a particularly successful strategy to push the *ZT* values beyond unity at high temperatures.[4,5]

Among the mechanisms that allow to manipulate the electronic bands beyond the rigid-like scheme, resonant levels (RLs) provide a textbook example.[3,4,5,6] Used as an efficient route to enhancing the thermopower of metals and semiconductors, a RL, or "virtual bound state",[7] may be formed upon doping a material at energies where a “real” bound state would be formed in the absence of neighboring atoms.[8] In the specific case of semiconductors, this resonant energy has to overlap with either the valence or the conduction bands. One of the manifestations of a resonant state is the formation of a sharp peak in the impurity’s density of electronic states

(DOS) at the resonance energy, leading to a distortion of the total DOS, the energy dependence of which varies rapidly over a narrow energy window. The hybridization of the resonant states with the host electronic states results in a band-smearing effect,[9,10,11] enabling an increase in the thermopower when the Fermi level resides near this distortion. Thus, the position of the RL with respect to the band edge and the width of the smeared bands are the key parameters to achieve optimized *ZT* values.

So far, the main experimental strategy to unravel the resonant nature of an impurity in semiconductors was tied to the variation of the thermopower α as a function of the charge carrier concentration *p*. Known as the Ioffe-Pisarenko plot, the $\alpha(p)$ relation is characteristic of the electronic structure of the host semiconductor, and is frequently well captured by models based on solutions of the Boltzmann transport equation. In most cases, doping induces a rigid-like shift of the Fermi energy in the conduction or valence bands, giving rise to smooth variations in $\alpha(p)$ that follow the Ioffe-Pisarenko plot of the host material. In contrast, the formation of a RL manifests as a significant departure from the predicted trend, signaling non-rigid-band behavior. Experimentally, the conclusion as for the resonant nature of the impurity can be drawn when the thermopower is significantly enhanced compared to the material specific $\alpha(p)$ curve, as observed for $Pb_{1-x}Tl_xTe$,[12,13] $Sn_{1-x}In_xTe$,[11,14] $Bi_{2-x}Sn_xTe_3$,[15] $As_{2-x}Sn_xTe_3$ [16] or $Ge_{1-x}In_xTe$.[17] However, upon doping, deviations from the rigid-band trend in $\alpha(p)$ may originate from other effects, such as variations in the dominant scattering mechanism or in the relative position of band extrema possibly leading to band convergence. Through substitutions or the formation of solid solutions, this last mechanism also efficiently enhances the *ZT* values due to the convergence of two, or more, band extrema that increases the number of valleys N_V and hence, the density-of-states effective mass m^*_{DOS} ($\alpha \propto m^*_{DOS} = N_V^{2/3} m^*_b$ where m^*_b is the band effective mass). Thus, an analysis of the character of an impurity solely based on the Ioffe-Pisarenko plot may be inconclusive. Here, we demonstrate a straightforward way of getting a

clear and independent experimental proof of the formation of a RL, allowing for the distinction between resonant and non-resonant impurities, regardless of their effect on the thermopower. Our analysis is based on a combination of low-temperature electrical and galvanomagnetic measurements to probe the emergence of resonant scattering, a mechanism specific to the presence of a RL[18,19] but not generally used to establish the resonant nature of an impurity. By performing systematic experimental and theoretical studies on the binary SnTe, we propose a novel methodology based on the construction of the compositional dependence of the residual resistivity $\rho_0(x)$ and charge carrier mobility $\mu_0(x)$, analogue to the Ioffe-Pisarenko plot. We hereafter consider the *p*-type chalcogenide semiconductor SnTe doped with the resonant impurity In[11,14] and the non-resonant impurities I, Ga, and Mn chosen as counter-examples. As a further proof-of-principle, the analysis for SnTe is supplemented by a similar one performed for the best-known resonant thermoelectric system $Pb_{1-x}Tl_xTe$.

Results and discussion

Figure 1 shows the Ioffe-Pisarenko plot of SnTe calculated using a two-valence band model[20, 21] (see Supplementary Information file for the equations and physical parameters used). The thermopower measured for self-doped and iodine-doped SnTe samples generally follows the model prediction. "Self-doped" samples correspond to pristine binary SnTe samples that contain naturally-formed defects, which are Sn vacancies acting as double-hole acceptors.[22,23,24,25] This behavior suggests that both the Sn vacancies and iodine substitutional impurity modify the valence band structure of SnTe in a rigid-like manner. In contrast, a substantial enhancement of the α values above the Ioffe-Pisarenko line is observed experimentally for In-, Mn-, and Ga-doped samples. Although all these three elements lead to a basically similar enhancement of α, different mechanisms are at play: In forms a resonant

level, while Mn induces band convergence of the two main valence bands governing the transport in SnTe,[26, 27] similarly to Ga, reported to increase the number of degenerate valleys in the Brillouin zone.[28] Thus, SnTe is an excellent and sensitive test-case to our proposed methodology, not only capable of confirming the resonant behavior of In but also to provide a clear distinction between In and non-resonant Ga/Mn, as the analysis solely based on thermopower enhancement is inconclusive.

The key difference between resonant and non-resonant impurities, serving as a basis for our methodology, is the distinct way with which they affect the electronic bands. To visualize this effect, a magnification of the electronic band structure of SnTe containing different doping atoms, is shown in **Figure 2** in the region of interest in the Brillouin zone (BZ; see **Figure S1** in **Supplementary Information**). Electronic structure calculations were performed using the KKR-CPA method[29,30], with the band structure being visualized using the Bloch spectral density functions (BSF), further details of which are given in the **Supplementary Information**. **Figure 2a** shows the valence bands of SnTe with 0.32% of Sn vacancies. This concentration of vacancies, inherent to SnTe, is equivalent to a hole concentration p of 10^{20} cm^{-3} as typically observed experimentally. SnTe samples are thus self-doped by Sn vacancies, which act as intrinsic rigid-band-like dopants, that is, they change the position of the Fermi energy but do not significantly modify either the density of states (DOS) or the electronic dispersion relations, inducing only a small band smearing (see below). In **Figure 2b,d** the valence band structure is shown with an additional doping of 0.5% of In and I. The difference between rigid-band-like (Sn vacancies and I) and resonant (In) doping is evident. Resonant state is formed on 5*s* orbitals of In, which is evidenced by **i)** the formation of a narrow peak in the partial In DOS; **ii)** an increased total DOS near the valence band edge, and **iii)** a strong valence band smearing. All these effects are intensified when the concentration of In increases, as presented in **Figure 2c.** In contrast, iodine (**Figure 2d**), being a monovalent donor in SnTe,[21] only rigidly shifts E_F

towards the valence band edge, compensating the acceptor behavior of Sn vacancies. Furthermore, while Ga (**Figure 2e,f**) is isoelectronic to In, it does not form RL but slightly increases the DOS near E_F and reduces the energy offset between the two band extrema at the L and Σ points, due to its non-rigid-like behavior.

Band smearing is an effect of prime importance to understand the difference in the transport properties between resonantly and non-resonantly doped samples. A deeper analysis of the dopant-induced band smearing is shown in **Figure 3**, in which we compare the shape of the last valence band, lying between the L and Σ points of the BZ (panels a-c and g-i). Thanks to the BSF technique, the strength of the band smearing, which is proportional to the strength of electron scattering on impurities, may be quantified. In a typical alloy systems, the BSF for a single wave vector $\boldsymbol{k}$ adopts the shape of the Lorentz function (see, Supplementary Information), and the electronic relaxation time τ is in such a case related to its full width at half maximum[31] Δ as $\tau = \frac{\hbar}{\Delta}$. In Figure 3(d-f) and (j-l) the BSF is plotted for $\boldsymbol{k}_1 \approx$ (0.469, 0.469, 0.00) $\frac{2\pi}{a}$ (a is the lattice parameter of the cubic crystal structure of SnTe), equivalent to 1/4 of the L − Σ distance, that is, near the point where the valence band is crossing the Fermi level E_F in panel a). Points show the calculated BSF while the line is a fit to a Lorentzian function. As shown in **Figure 3d,j**, the Lorentzian describes very well the shape of the BSF when non-resonant impurities (Sn vacancies and I) are present, with a magnitude of the relaxation time of $\tau \sim$ 3-4×10^{-13} s at $\boldsymbol{k}_1$. Slightly larger smearing is induced by Ga (**Figure 3h-i,k-l**), but still a Lorentzian character of BSF is retained, even for 2% of Ga. In sharp contrast, the addition of a minute amount of In as low as 0.5% is sufficient to generate a non-Lorentzian BSF with shoulders. Such a modification is characteristic of resonant levels[8,9] and strongly enlarge the width of the BSF. This effect is dramatically enhanced upon increasing the In concentration to 2% for which the BSF exhibits a double-bell shape. Rough estimates of τ at the same $\boldsymbol{k}_1$-point

drops to 2×10^{-14} s for 0.5% In, and to 3×10^{-15} s for 2% In, *i.e.* an order of magnitude lower than that of Ga and two orders of magnitude lower than those obtained for Sn vacancies and I. This huge difference in τ opens the possibility of an experimental detection of RL through electrical transport measurements since the electric conductivity σ and carrier mobility μ are inversely proportional to τ. Moreover, our results clearly show that the relaxation time is no longer well-defined for such non-Lorentzian BSF shapes,[31] resulting in differences in actual mobilities that will be even larger than differences in τ suggest. To precisely quantify the effect of impurity-induced scattering and take into account the contributions from the whole Brillouin zone, electric conductivity needs to be calculated. Due to the strong smearing of the electronic bands, the Boltzmann formalism within the relaxation time approximation would fail to describe appropriately the transport properties of this system, due to the impossibility to derive the velocity of the charge carriers defined as the gradient of the band energy with respect to the wave vector. These difficulties can be overcome by using the Kubo-Greenwood formalism[29,31,32,33] that enables to calculate the residual electrical resistivity and charge carrier mobility at the temperature of 0 K, taking into account the impurity-induced scattering. The comparison of calculations with measurements performed at liquid helium temperatures, that is, in the limit where impurity scattering largely outweighs phonon scattering, may thus clearly distinguish between resonant and non-resonant impurities. **Figure 4** shows such comparison with the electrical resistivities ρ_0 and hole mobilities μ_0 measured at 5 K in the series of polycrystalline samples $Sn_{1.03-x}In_xTe$ ($0 \leq x \leq 0.02$) reported as a function of the In concentration (the excess Sn concentration introduced in the nominal composition was used to partly compensate the formation of Sn vacancies, further experimental details and numerical values are gathered in **Supplementary Information**). In calculations, the experimental and theoretical hole concentrations were matched by adding an appropriate number of Sn vacancies, which act as double-hole acceptors (all the data are gathered in **Table 1)**. The comparison of the

theoretical and experimental ρ_0 values indicates an overall good agreement between both sets of data. In particular, the calculations capture qualitatively the two main characteristics of ρ_0, that is, its linear increase with increasing x for substitution levels lower than 1% and its tendency to level off at higher In concentrations. Furthermore, below 0.5%, the computed values agree quantitatively with the experimental data while above this concentration, the calculations tend to overestimate the experimental values, most likely due to overestimation in the density-of-states effective mass, as discussed in Ref. [11].

A straightforward visualization of the strong scattering of holes on the RL is provided by the rapid decrease in the hole mobility μ_0 measured by Hall effect (**Figure 4b**). Despite the very low substitution levels covered in the series $Sn_{1.03-x}In_xTe$, μ_0 drops by two orders of magnitude from 3405 $cm^2\ V^{-1}\ s^{-1}$ for $x = 0.0$ to 34 $cm^2\ V^{-1}\ s^{-1}$ for $x = 0.02$. This trend is well captured by our calculations over the entire concentration range, which confirms that it is an intrinsic property of the material, related to the RL. Note that the polycrystalline nature of our samples results in grain boundary scattering that contributes to limit the hole mobility in the $x = 0$ sample, which is likely the reason for the larger disagreement between calculations and measurements in this case. Nevertheless, the overall agreement achieved herein suggests that this mechanism only weakly influences μ_0 at very low temperatures compared to resonant scattering. It is important to recall here that the strong reduction in mobility at such a low temperature does not rule out the beneficial influence of the RL on enhancing the thermoelectric properties at high temperatures. Above room temperature, the strengths of the electron-phonon and temperature-independent RL scattering start to be of similar magnitudes, significantly reducing the difference in mobilities between resonantly- and non-resonantly-doped SnTe. In particular, as shown in Ref. [11], the ratio of electrical resistivities of 2% In doped and 0% In doped SnTe samples dropped to only 1.3 at 800 K, leading to comparable mobilities in both samples. This allows for an enhancement in the peak ZT values in SnTe with resonant In

dopant,[11,14] in spite of the low-temperature reduction in mobility. Moreover, due to the lower sensitivity of resonant-doped system on temperature-induced electron-phonon scattering when compared to non-resonant doping, the *ZT* enhancement was observed to persist in a broader temperature range, leading to enhanced average *ZT* values.[11] Similar situation was also evidenced in Tl-doped PbTe.[13]

The benefit of constructing residual resistivity $\rho_0(x)$ and residual mobility $\mu_0(x)$ plots becomes evident when comparing the above-mentioned trends with those of I and Ga-doped SnTe (only calculated values because no low-temperature resistivity measurements are available in literature), as well as Mn-doped SnTe (calculated and experimental[34,35,36,37] values, see also Figure S3 in the Supplementary Information file for an additional mobility plot for Mn-doped SnTe with a constant vacancy concentration). Despite the similar substitution levels in all the four series of samples, In induces a striking enhancement in ρ_0 and reduction in μ_0 compared to the rigid-band-like I and non-rigid-band-like, non-resonant Mn and Ga dopants, clearly highlighting the resonant character of In in SnTe. Thus, the $\rho_0(x)$ and $\mu_0(x)$ plots provide a direct and convenient visualization of the resonant nature of In while an analysis solely based on the Ioffe-Pisarenko plot would remain inconclusive in this case.

To successfully apply this methodology to new semiconductors and impurities of an unknown character, more than two different series of samples should be considered, paying a particular attention to the low impurity concentration range. As seen in Fig. 4, the drop of $\mu_0(x)$ and increase in $\rho_0(x)$ for SnTe are the steepest up to 1% of impurity concentration. In this compositional range, the difference between the rigid-band-like I and non-rigid, non-resonant Ga and Mn (which scatter more strongly than I) is not very pronounced, below an order of magnitude, in contrast to the two-orders-of-magnitude difference between I and In.

It is important to emphasize that $\mu_0(x)$ is a more sensitive indicator of the presence of a RL compared to the enhancement in α typically observed in the Ioffe-Pisarenko plot, as the

difference between RL and non-RL doping cases reaches one-to-two orders of magnitude. Moreover, the sole electrical resistivity analysis could be also misleading for impurities that compensate the main charge carriers, as is the case of I that behaves as a donor impurity in *p*-type SnTe. The relatively rapid increase in ρ_0 with x seen for I-doped SnTe in **Figure 4a** is mainly caused by the decrease in the hole concentration (see **Table 1**), rather than by the appearance of strong scattering, as evidenced by the weak $\mu_0(x)$ dependence (see **Figure 4b).** Thus, both physical quantities should be analyzed in parallel to draw firm conclusions.

Furthermore, the methodology proposed herein should be used to analyze the mobility in samples doped with similar impurity and charge carrier concentrations, and for which, scattering on point-defects (*i.e.* on impurities) is the main source of electrical resistivity in addition to phonon scattering. In particular, the ρ_0 and μ_0 values may be affected by both microstructural and disorder-related effects that notably include grain boundary scattering and the disorder induced by the dopants and possible intrinsic defects. For these reasons, this approach may not be applicable to nanostructured samples for which, the small grain size may be the dominant source of electrical resistance. Although concerns related to charge localization at the grain boundaries can be avoided by performing systematic studies on single crystals, our present results show that our proposed methodology is equally applicable to polycrystalline samples. As demonstrated in our prior study on the series $Sn_{1.03-x}In_xTe$,[11] the careful control of the synthesis process, and notably of the mass-to-volume ratio in the silica ampules, ensured very similar microstructure and Sn vacancy concentrations, resulting in the observed step-like variations in the transport properties over the In concentration range covered. The possible presence of energy barriers at the grain boundaries, observed in various chalcogenide semiconductors and giving rise to activated-like behavior of the Hall mobility, can be ruled out in the series $Sn_{1.03-x}In_xTe$ due to the conventional temperature dependences of the Hall mobility and the metallic character of the electrical resistivity (see **Figure S4 in Supplementary**

Information). In the specific case of SnTe, the very high dielectric constant of around 1700 (Ref. 38; G. Nimtz and B. Schlicht in Narrow-Gap Semiconductors (Springer, Berlin, 1983)) tends to strongly lessen the development of energy barriers at the grain boundaries.[44,45] In addition to intrinsic defects, dopants inevitably further enhance the level of disorder, which also decreases the charge carrier mobility in semiconductors. However, the comparison of the influence of In on the electrical resistivity and Hall mobility with those observed for other dopants shows that resonant scattering largely outweighs the effect of disorder.

The effectiveness of our methodology is further confirmed by literature results gathered for Tl- and Na-doped PbTe in **Figure 5**. Using available experimental data[38,39,40,41,42,43] we have constructed the residual resistivity and the residual mobility plots, which evidence the same behavior as in the case of SnTe. The resonant character of Tl against non-resonant Na is highlighted by the increase in $\rho_0(x)$ and decrease in $\mu_0(x)$ for similar impurity concentrations, and supplements the conclusion of the Tl resonance drawn from the Ioffe-Pisarenko plot and band structure calculations.[6,10,12]

Conclusions

In conclusion, we have shown that the compositional dependences of the residual electrical resistivity ρ_0 and charge carrier mobility μ_0 can provide a clear experimental signature of the resonant character of the introduced dopant in semiconductors. At low temperatures, both physical quantities successfully capture the fundamental differences between resonant and conventional doping impurities, despite both of them may lead to seemingly similar thermopower enhancements. This conclusion is firmly confirmed by calculations of the electrical conductivity of the resonant system $Sn_{1-x}In_xTe$ using the Kubo-Greenwood formalism that enabled us to make a direct connection between our experimental observations and the RL-induced resonant scattering that governs ρ_0 and μ_0 at low temperatures. The simple method of

constructing $\rho_0(x)$ and $\mu_0(x)$ plots, analogous to the Ioffe-Pisarenko plot, provides an independent tool to characterize the nature of a given impurity in semiconductors, in which scattering on impurities is the main source of the residual electrical resistivity. This reinforces the interest of probing the transport properties of doped semiconductors down to liquid helium temperatures.

Conflicts of interest

There are no conflicts to declare.

Acknowledgements

B.W. and S.M. have contributed equally to this work. B.W. was partly supported by the National Science Centre (Poland), project No. 2017/26/E/ST3/00119.

Table 1. Experimental and calculated values of the residual resistivity ρ_0 and residual mobility $\mu_0 = \frac{1}{\rho_0 p q_e}$ (q_e is the elementary charge, p is the measured Hall carrier concentration in the case of experimental data and a nominal carrier concentration in the case of calculated values) for SnTe doped with In, Mn, Ga (on Sn site), and I (on Te site), as a function of the dopant concentration x. The experimental values of p for the In series were measured at 5 K. Data are presented in Figure 4. Sn vacancy concentrations Vac_{Sn} were used in the calculations to match the experimental and theoretical hole concentrations. For SnTe doped with In and Mn, for which the experimental data were available, the hole concentration p in the calculations was fixed to the experimental value (shown in the second column) by adding an appropriate number of Sn vacancies, as shown in the last column. Each Vac_{Sn} acts as a double-hole acceptor, whereas In and Ga provide a single hole to SnTe, and Mn is a neutral impurity if substituted for Sn in SnTe (all the holes come from Vac_{Sn} in this case). For SnTe doped with Ga, for which we are not aware of any low temperature resistivity and carrier concentration measurements in the literature, a constant concentration of 0.5% of Sn vacancies was assumed. Experimental data for Mn were taken from Ref. [34] (all concentrations except for 1%, 2.2%, 3%), Ref. [35] for 1 and 3%, and Ref. [36] for 2.2%. From Ref. [34], data for annealed samples, available for $x \leq$ 0.88%, were taken. Experimental Hall carrier concentrations for I were taken from Ref. [21]. In the case of Mn-doped SnTe, due to transition to the ferromagnetic state, an anomaly in the electrical resistivity is observed at low temperatures [34]. However, this anomaly only changes the electrical resistivity by few percent, so that it does not affect our conclusions.

x (%)	p (10^{20} cm^{-3})	ρ_0 exp. ($\mu\Omega$ m)	ρ_0 calc. ($\mu\Omega$ m)	μ_0 exp. (cm^2 V^{-1}s^{-1})	μ_0 calc. (cm^2 V^{-1}s^{-1})	% Vac_{Sn}
			In			
0.00	1.05	0.19	0.09	3400	6558	0.33
0.05	1.41	0.33	0.26	1440	1702	0.42
0.15	1.63	0.78	0.61	547	627	0.44
0.25	1.76	1.12	1.06	316	335	0.43
0.35	2.14	1.52	1.24	195	235	0.50
0.45	2.14	1.85	1.94	160	150	0.45
0.60	2.35		3.16		84	0.44
0.75	2.58	3.26	4.15	83	58	0.44
0.85	2.61		5.21		46	0.40
1.00	2.76	3.19	5.94	73	38	0.37
1.50	3.55		5.95		30	0.37
2.00	4.50	4.08	5.41	32	26	0.42
2.50	5.23		5.13		23	0.40
3.00	6.02		4.81		22	0.40
			Mn			
0.04	1.70	0.20	0.14	1800	2585	0.41
0.13	1.40	0.18	0.16	2510	2723	0.44
0.22	2.10	0.25	0.21	1175	1430	0.66
0.35	1.50	0.23	0.25	1829	1690	0.47
0.44	1.20	0.26	0.29	1996	527	0.38
0.88	2.80	0.36	0.45	617	527	0.88
1.00	2.66	0.27	0.45	870	527	0.84
1.50	2.54		0.58		422	0.80
2.20	2.87	0.36	0.75	600	289	0.91
3.00	3.14	0.86	0.93	231	214	0.99
			Ga			
0.00	1.58		0.12		3329	0.50
0.50	2.38		0.15		1774	0.50
1.00	3.17		0.15		1287	0.50
1.50	3.96		0.15		1057	0.50
2.00	4.75		0.16		847	0.50
2.50	5.55		0.16		721	0.50
3.00	6.34		0.16		608	0.50
			I			
0.50	0.82		0.25		3054	0.51
1.00	0.60		0.45		2303	0.69
1.50	0.35		0.82		2183	0.86
2.00	0.32		1.00		1969	1.10

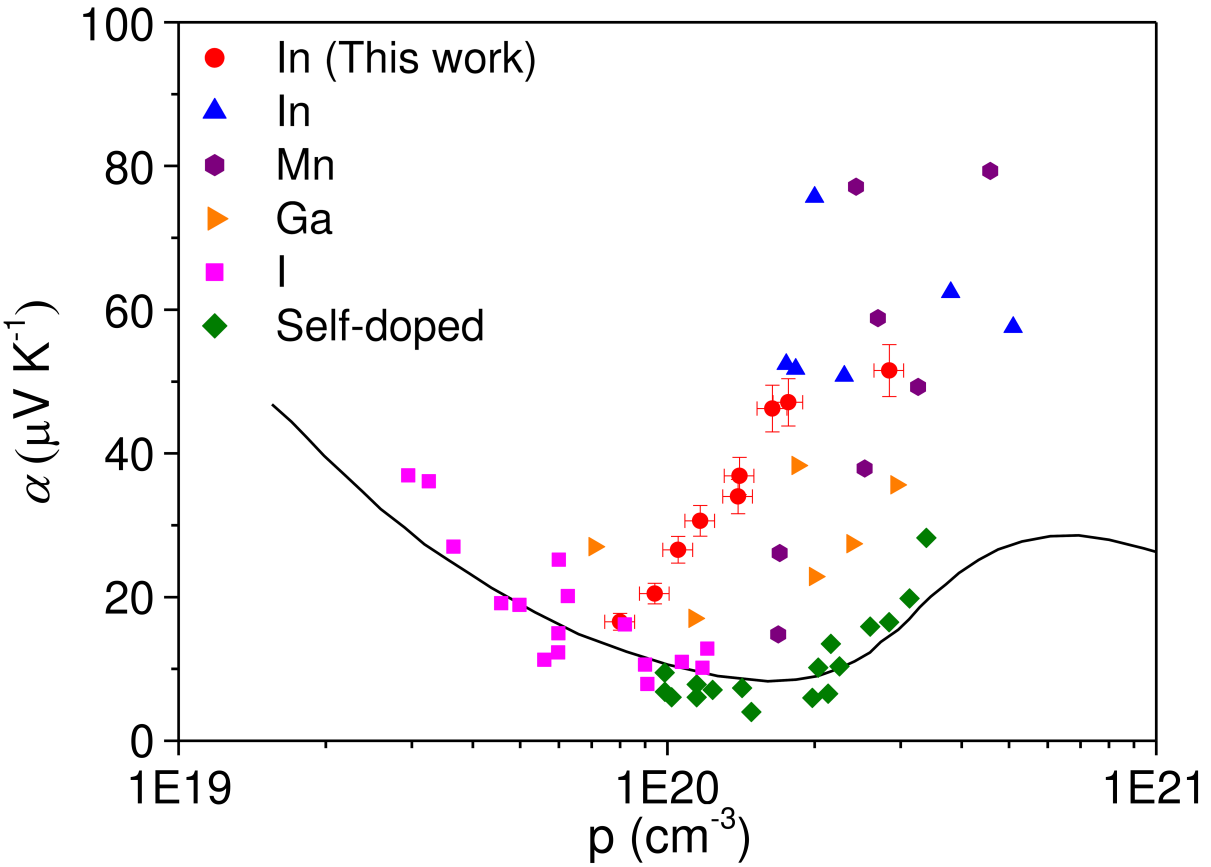

Figure 1. Ioffe-Pisarenko plot of SnTe showing variations in the thermopower α as a function of the hole concentration p. The black solid curve stands for the theoretical dependence calculated using a two-valence-band model.[11,21,23] The experimental data points are taken from the literature for In-doped,[11,14], I-doped,[21] Mn-doped,[27] Ga-doped,[28] and self-doped (that is, by Sn vacancies)[14,22,23] SnTe samples.

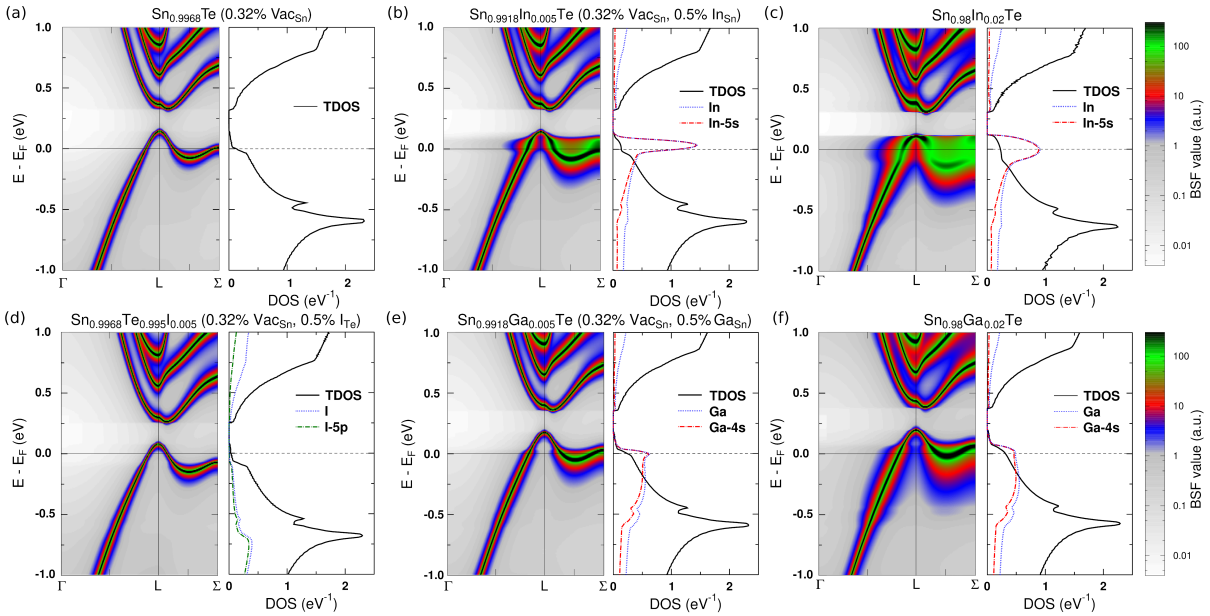

Figure 2. Density of states (DOS) and electronic band structure around the L point of the Brillouin zone (see Figure S1 in Supplementary Information) based on Bloch spectral functions (BSF) of SnTe doped with: (a) 0.32% of Sn vacancies (Vac_{Sn}); (b) 0.32% of Vac_{Sn} and 0.5% of In_{Sn}; (c) 2% of In_{Sn}; (d) 0.32% of Vac_{Sn} and 0.5% of I_{Te}; (e) 0.32% of Vac_{Sn} and 0.5% of Ga_{Sn}; (f) 2% of Ga_{Sn}. TDOS is the total DOS per formula unit, whereas dotted and dashed lines show partial DOS of impurity atoms with their dominating angular momentum contribution, calculated per atom (that is, not multiplied by its concentration).

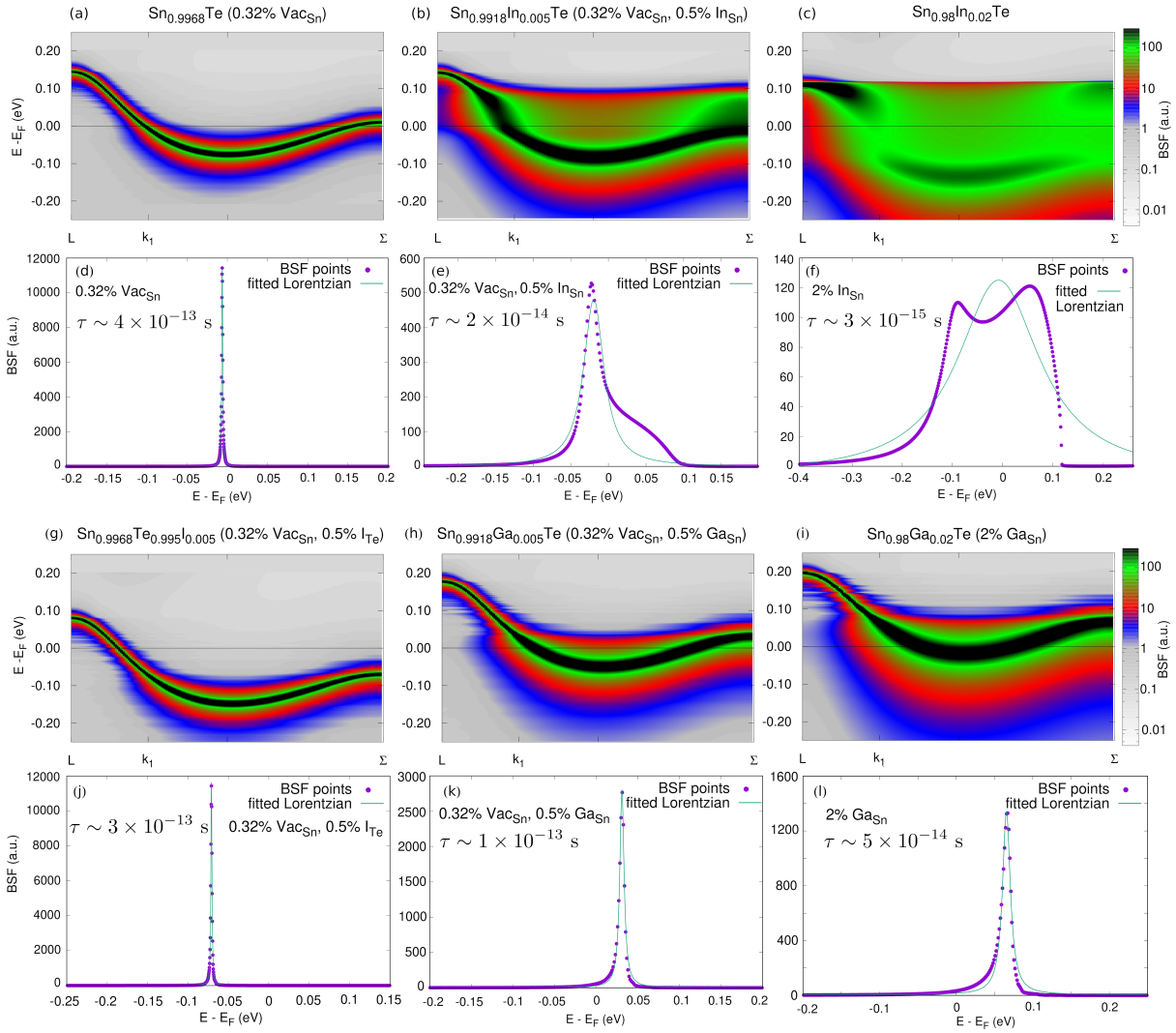

Figure 3. (a-c, g-i) Two-dimensional projections of Bloch spectral functions (BSF), plotted in logarithmic scale, for the last valence band between the L and Σ points of the Brillouin zone for SnTe containing (a) 0.32% of Vac_{Sn}; (b) 0.32% of Vac_{Sn} and 0.5% of In_{Sn}; (c) 2% of In_{Sn}; (g) 0.32% of Vac_{Sn} and 0.5% of I_{Te}; (h) 0.32% of Vac_{Sn} and 0.5% of Ga_{Sn}; (i) 2% of Ga_{Sn}. In these plots, the black color corresponds to a BSF value greater than 300 a.u., that is, 22 eV^{-1}. In panels (d-f) and (j-l) the BSF is plotted for $k_1 \approx (0.469, 0.469, 0.00)\ \frac{2\pi}{a}$ (a is the lattice parameter of the cubic crystal structure of SnTe), equivalent to 1/4 of the L − Σ distance, that is, near the point where the valence band is crossing the Fermi level in panel a). Points show the calculated BSF while the line is a fit to a Lorentzian function. While the fit is very good in the non-resonant case, the Lorentzian function is no longer a good approximation of the BSF shape in e) and especially f). The electronic lifetime, estimated from the width of the fitted Lorentzian, is shown in the figures.

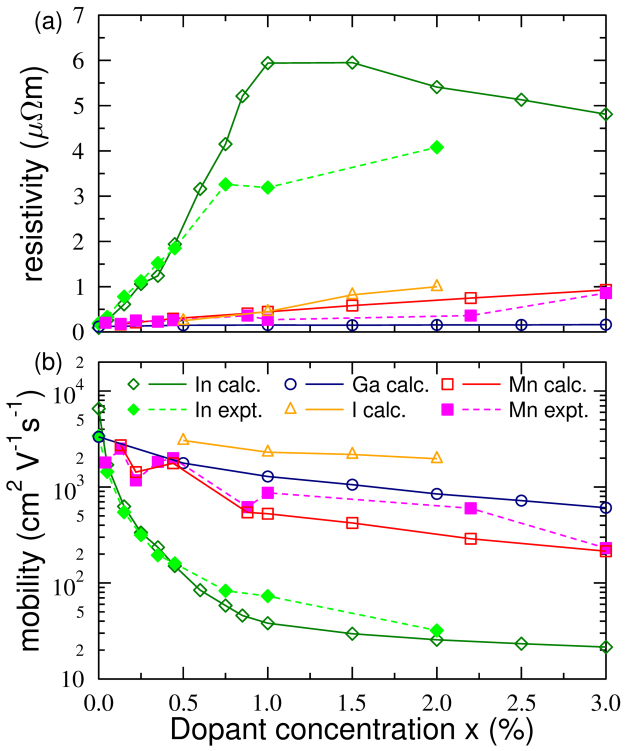

Figure 4. (a) Residual electrical resistivity ρ_0 and (b) residual hole mobility μ_0 as a function of the dopant concentration x in SnTe. In calculations for In, I and Mn cases, hole concentrations were fixed to the experimental values by adding an appropriate concentration of Sn vacancies (ranging from 0.4 up to 1%), each of them acting as a double-hole acceptor (see **Table 1**). For Ga, a concentration of 0.5% of Sn vacancies was kept constant across the entire Ga concentration range. The data measured on single-crystalline and polycrystalline Mn-doped SnTe were taken from Refs. [34,35,36], where they were measured at temperatures below 5 K. In panel (a) lines and symbols are the same as in panel (b). Lines are guides to the eye in both panels.

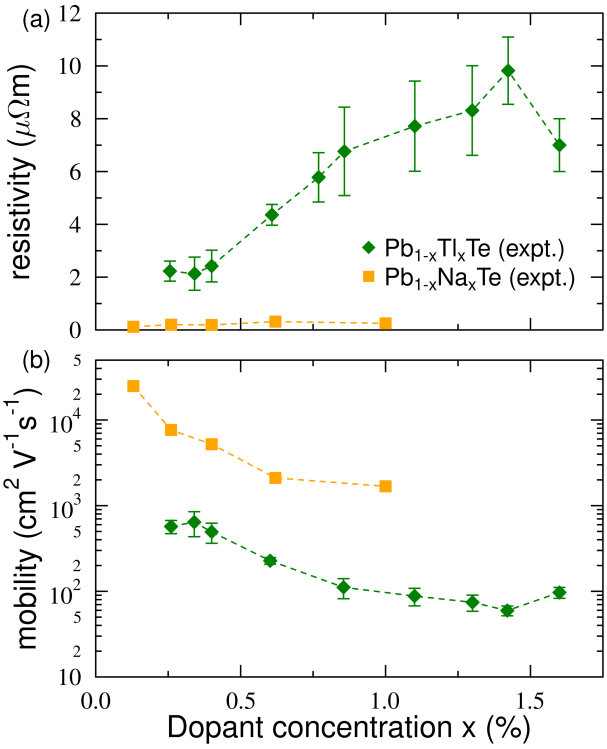

Figure 5. Residual resistivity $\rho_0(x)$ and residual mobility $\mu_0(x)$ plots for PbTe doped with resonant impurity Tl and non-resonant impurity Na. Experimental data were taken at temperatures below 4 K in Refs.: [38] (for Na concentrations of up to 0.62%), [39] (1% Na), [40,41,42] (Tl concentrations up to 1.4%), [43] (1.6% Tl). Relatively large error bars for the electrical resistivity in $Pb_{1-x}Tl_xTe$ are taken after [42], for 1.6% Tl-doped PbTe the error bar has been estimated from the point size in Ref. [43]. Enhancement of $\rho_0(x)$ and drop in $\mu_0(x)$ are similar to those observed for SnTe:In versus SnTe:Mn, SnTe:Ga, and SnTe:I, confirming the ability of the residual resistivity and residual mobility plots to distinguish between resonant and non-resonant impurities, in addition to the Ioffe-Pisarenko plot.

References

[1] Goldsmid, H. J. in *Thermoelectric Refrigeration*; Springer: New York, 1964.
[2] Thermoelectrics and its Energy Harvesting, edited by D. M. Rowe, CRC Press, Boca Raton, FL, USA 2012.
[3] T. Zhu, Y. Liu, C. Fu, J. P. Heremans, J.G. Snyder, X. Zhao, *Adv. Mater.* 2017, **29**, 1605884
[4] Y. Pei, H. Wang, G.J. Snyder, *Adv. Mater*. 2012, **24**, 6125.
[5] Advanced Thermoelectrics: Materials, Contacts, Devices, and Systems, ed. Z. Ren, Y. Lan, Qi. Zhang, CRC Press, Boca Raton, FL, USA 2018.
[6] J. P. Heremans, B. Wiendlocha, A. M. Chamoire, *Energy Environ. Sci.* 2012, **5**, 5510.
[7] J. Friedel, Can. J. Phys. 1956, **34**, 1190.
[8] B. L. Györffy and G. M. Stocks, in *Electrons in disordered metals and metallic surfaces*, (Eds. P. Phariseau, B.L. Györffy and L. Scheive). NATO ASI Series, Physics, B42. Plenum Press, NY, **1979**.
[9] B. Wiendlocha, *Phys. Rev. B* 2013, **88**, 205205.
[10] B. Wiendlocha, *Phys. Rev. B* 2018, **97**, 205203.
[11] S. Misra, B. Wiendlocha, J. Tobola, F. Fesquet, A. Dauscher, B. Lenoir, C. Candolfi, *J. Mater. Chem. C* 2020, **8**, 977.
[12] J. P. Heremans, V. Jovovic, E. S. Toberer, A. Saramat, K. Kurosaki, A. Charoenphakdee, S. Yamanaka, G. J. Snyder, Science 2008, **321**, 554.
[13] Christopher M. Jaworski, Bartlomiej Wiendlocha, Vladimir Jovovic and Joseph P. Heremans, *Energy Environ. Sci.*, 2011, **4**, 4155
[14] Q. Zhang, B. Liao, Y. Lan, K. Lukas, W. Liu, K. Esfarjani, C. Opeil, D. Broido, G. Chen and Z. Ren, *Proc. Natl. Acad. Sci. USA* 2013, **110**, 13261.
[15] C. M. Jaworski, V. Kulbachinskii and J. P. Heremans, *Phys. Rev. B* 2009, **80**, 233201.
[16] B. Wiendlocha, J.-B. Vaney, C. Candolfi, A. Dauscher, B. Lenoir and J. Tobola, *Phys. Chem. Chem. Phys.* 2018, **20**, 12948.
[17] L. Wu, X. Li, S. Wang, T. Zhang, J. Yang, W. Zhang, L. Chen, J. Yang*, NPG Asia Materials* 2017**, 9**, e343.
[18] V.I. Kadanov, Y.I. Ravich, *Sov. Phys. Usp.* 1985**, 28***,* 31.
[19] Y.I. Ravich, in *CRC Handbook of Thermoelectrics* (Ed. D. M. Rowe), CRC Press, Boca Raton, FL, USA 2012.
[20] R. F. Brebrick and A. J. Strauss, *Phys. Rev*. 1963, **131**, 1043
[21] M. Zhou, Z. M. Gibbs, H. Wang, Y. Han, C. Xin, L. Li, G.J. Snyder, *Phys. Chem. Chem. Phys.* 2014,**16**, 20741.
[22] R. F. Brebrick, A. J. Strauss, *J. Chem. Phys.* 1964, **41**, 197.
[23] L. M. Rogers, *J. Phys. D: Appl. Phys.* 1968, **1**, 845.
[24] D. Ibrahim, C. Candolfi, S. Migot, J. Ghanbaja, A. Dauscher, G. Le Caër, B. Malaman, C. Semprimoschnig, B. Lenoir, *Phys. Rev. Mater.* 2019, **3**, 085404.
[25] D. Ibrahim, S. Misra, S. Migot, J. Ghanbaja, A. Dauscher, B. Malaman, C. Semprimoschnig, C. Candolfi, B. Lenoir, *RSC Adv.* 2020, **10**, 5996.
[26] G. Tan, F. Shi, S. Hao, H. Chi, T. P. Bailey, L.-D. Zhao, C. Uher, C. Wolverton, V. P. Dravid, M. G. Kanatzidis, *J. Am. Chem. Soc.* 2015, **137**, 11507.
[27] W. Li, J. Tang, X. Zhang, Y. Pei, in *Novel Thermoelectric Materials and Device Design Concepts* (Eds. S. Skipidarov, M. Nikitin), Springer Nature Switzerland AG, **2019.**
[28] R. Al Rahal Al Orabi, J. Hwang, C.-C. Lin, R. Gautier, B. Fontaine, W. Kim, J.-S. Rhyee, D. Wee, M. Fornari, *Chem. Mater.* 2017, **29**, 612.
[29] H. Ebert, D. Ködderitzsch, J. Minár, *Rep. Prog. Phys.* 2011, **74**, 096501.

[30] H. Ebert *et al.*, The Munich SPR-KKR package, version 7.7.3, **2019**. https://www.ebert.cup.uni-muenchen.de/index.php/en/software-en/13-sprkkr (accessed on 04.03.2021)
[31] W. H. Butler, *Phys. Rev. B* 1985**, 31**, 3260.
[32] R. Kubo, *J. Phys. Soc. Jap.* 1957, **12**, 570.
[33] D. A. Greenwood, *Proc. Phys. Soc.* 1958, **71**, 585.
[34] M. Inoue, H. Yagi, K. lshii, T. Tatsukawa *J. Low Temp. Phys.* 1976**, 23***,* 785.
[35] H. Chi, G. Tan, M.G. Kanatzidis, Q. Li, C. Uher, *Appl. Phys. Lett.* 2016, **108**, 182101.
[36] M. Inoue, K. lshii, H. Yagi, T. Tatsukawa, *Memoirs of the Faculty of Engineering, Fukui University*, 1976, **24**, 237.
[37] Note that the scattered and non-monotonic evolution of μ_0 at low x for $Sn_{1-x}Mn_xTe$ is related to large variations in the Sn vacancy concentrations from sample to sample, maintained also in our calculations. In Figure S3, we show additionally calculated mobilities for the fixed 0.5% Sn vacancy concentration, where the evolution of μ_0 with x is smooth and monotonic.
[38] P. Giraldo-Gallo, B. Sangiorgio, P. Walmsley, H. J. Silverstein, M. Fechner, S. C. Riggs, T. H. Geballe, N. A. Spaldin, I. R. Fisher, *Phys. Rev. B* 2016, **94**, 195141.
[39] C. M. Jaworski, M. D. Nielsen, H. Wang, S. N. Girard, W. Cai, W. D. Porter, M. G. Kanatzidis, J. P. Heremans, *Phys. Rev. B* 2013, **87**, 045203.
[40] M. Matusiak, E.M. Tunnicliffe, J. R. Cooper, Y. Matsushita, I. R. Fisher, *Phys. Rev. B* 2009, **80**, 220403.
[41] Y. Matsushita, P. A. Wianecki, A. T. Sommer, T. H. Geballe, I. R. Fisher, *Phys. Rev. B* 2006, **74**, 134512.
[42] Y. Matsushita, Superconductivity and mixed valency in thallium doped lead telluride, *Ph.D. Thesis*, Stanford University, USA, 2007. https://web.stanford.edu/group/fisher/people/Yana_Matsushita_thesis.pdf (accessed on 04.03.2021)
[43] T. Keiber, F. Bridges, B. C. Sales, H. Wang, *Phys. Rev. B* 2013*,* **87**, 144104.